Supporting Information

Ultrafast Control of Terahertz Harmonic Generation by optically modulating carrier dynamics in nonlinear metasurfaces

Zhehao Ye[2], Yongzheng Wen[1, *], Chen Wang[1], Yong Tan[1], Renfei Zhang[3], Fuli Zhang[2, *], Yuancheng Fan[2], Ji Zhou[1, *]

1 *State Key Laboratory of New Ceramic Materials, School of Materials Science and Engineering, Tsinghua University, Beijing 100084, China;*

2 *MOE Key Laboratory of Material Physics and Chemistry under Extraordinary Conditions, School of Physical Science and Technology, Northwestern Polytechnical University, Xi'an 710129, China;*

3 *Research Center for Metamaterials, Wuzhen Laboratory, Jiaxing 314500, China;*

*Corresponding authors: wenyzheng@tsinghua.edu.cn (Yongzheng Wen); fuli.zhang@nwpu.edu.cn (Fuli Zhang); zhouji@tsinghua.edu.cn (Ji Zhou);

Received 09 October 2025; Revised 25 November 2025; Accepted XX 2025; Published online XX 2025

Contents

S1 Theory of second and third harmonic generation

S2 Simulations of the THz metasurfaces

S3 Experimental setup

S4 The dependence of SHG and THG on the optical pump energy density

S5 Second and third-order susceptibility

S6 Intervalley scattering

S7 The influence of thermal accumulation

References

S1 Theory of second and third harmonic generation

When intrinsic GaAs is illuminated by 800 nm laser radiation, each photon carries energy that can be described as

$$E_{\text{photon}} = \frac{\hbar c}{\lambda} = \frac{1240\text{eV} \cdot \text{nm}}{800\text{nm}} = 1.55\text{eV} \tag{S1}$$

Since this exceeds GaAs's direct bandgap (E_g=1.42 eV at 300 K), photons are absorbed through fundamental interband transitions. Electrons in the valence band are excited to the conduction band. The high absorption coefficient ($\alpha \sim 10^4 \text{ cm}^{-1}$) enables efficient carrier generation within the penetration depth 1 μm [1].

Second harmonic generation

The photoexcited free electrons' motion in pumped-GaAs of metasurfaces under strong electromagnetic fields can be described with a modified Drude model as

$$\mathrm{m}^* \frac{d^2\vec{r}}{dt^2} + \mathrm{m}^*\gamma \frac{d\vec{r}}{dt} = \mathrm{q}\vec{E}e^{-i\omega t} + \mathrm{q}\,v \times \vec{B}e^{-i\omega t} + c.c. \tag{S2}$$

Where, m^* denotes the effective mass of the electrons, γ denotes collision rate of the electrons, $\vec{r}$ denotes the motion of the electrons, q denotes the elementary charge, ω denotes the fundamental angular frequency, t is time, v denotes the velocity of the electrons, $\vec{E}$ denotes the amplitude of the local electric field, $\vec{B}$ denotes the amplitude of the local magnetic field, and c.c. denotes the complex conjugate term.

The drift velocity of free electrons determined by the local electric field can be expressed as:

$$v = i\mu_e \vec{E}e^{-i\omega t} \tag{S3}$$

Where μ_e denotes the complex mobility of the electrons.

Combining the equations (S3), the equation (S2) can be described as:

$$\mathrm{m}^* \frac{d^2\vec{r}}{dt^2} + \mathrm{m}^*\gamma \frac{d\vec{r}}{dt} = \mathrm{q}\vec{E}e^{-i\omega t} + i\mathrm{q}\mu_e \vec{E} \times \vec{B}e^{-i2\omega t} + c.c. \tag{S4}$$

The second-order term in the right arises from the electromagnetic contribution denotes the contribution of the Lorentz force, which drives the free electrons oscillating in an anharmonic way.

The solution of the equation can be solved by assuming a general solution as $\vec{r} = \vec{r}_\omega e^{-i\omega t} + \vec{r}_{2\omega} e^{-i2\omega t} + c.c.$.

$$\vec{r}_{\omega} = \frac{q\vec{E}}{\mathrm{m}^{*}(\omega^{2} - i\omega\gamma)} \tag{S5}$$

$$\vec{r}_{2\omega} = \frac{q\mu_{e}\vec{E}\times\vec{B}}{\mathrm{m}^{*}(4\omega^{2} - i2\omega\gamma)} \tag{S6}$$

Where $\vec{r}_{\omega}$ denotes the displacement driven by the local field with fundamental angular frequency ω, and $\vec{r}_{2\omega}$ denotes the displacement of the electrons driven by the Lorentz force with twice the fundamental frequency 2ω.

According to the definition of the polarization density, the second-order polarization ($P_{2\omega}$) can be obtained as:

$$P_{2\omega} = \frac{\iiint_{V} qn_{e}r_{2\omega}\mathrm{d}V}{V} \tag{S7}$$

Where n_{e} denotes the density of the photoexcited free electrons, V denotes the volume of pumped GaAs, where has second-order nonlinearity.

By assuming an average M and N times enhancement of the local electric and magnetic fields with respect to the incident THz electric fields. The equation (S7) can be written as:

$$p_{2\omega} = -\frac{q^{2}MN\langle n_{e}\rangle\langle\mu_{e}\rangle E_{i}^{2}}{c_{0}m^{*}\left(2\omega\gamma - i4\omega^{2}\right)} \tag{S8}$$

Where, $\langle n_{e}\rangle$ and $\langle\mu_{e}\rangle$ are average density and complex mobility of the free electrons, respectively, E_i is the amplitude of the incident terahertz electric field, and c_0 is the speed of light in vacuum.

According to the definition of polarization density $P_{2\omega} = \varepsilon_{0}\chi^{(2)}E_{i}\cdot E_{i}$, where ε_{0} denotes the vacuum permittivity, and $\chi^{(2)}$ denotes the effective second-order susceptibility.

$$\chi^{(2)} = -\frac{q^{2}MN\langle n_{e}\rangle\langle\mu_{e}\rangle Z_{0}}{m^{*}\left(2\omega\gamma - i4\omega^{2}\right)} \tag{S9}$$

Where Z_{0} denotes the free space impedance.

According to the equation (S9), the effective second-order nonlinear coefficient scales critically with material parameters: high electron density, large carrier mobility, reduced effective mass, and significant field enhancement induced by metamaterial structuring collectively amplify nonlinear responses. By temporally synchronizing optical pumping with terahertz excitation to control the dynamics of carriers, ultrafast switching functionality can be realized. Furthermore, through pump power tuning, we can actively manipulate carrier concentration and mobility profiles, thereby enabling continuous amplitude modulation of second-harmonic signals.

Third harmonic generation

For intrinsic GaAs without illumination with 800 nm pump, electrons predominantly reside in the covalently bound states within the valence band. Due to GaAs possessing a bandgap substantially exceeding terahertz photon energy, inter-band transitions contribute negligibly to THz nonlinearities. However, under above-bandgap photoexcitation with 800 nm laser, electrons are promoted from the valence to the conduction band, generating high-density non-equilibrium electron-hole pairs. Terahertz waves can efficiently drive intra-band transitions of these photoinduced carriers, accelerating conduction-band electrons and valence-band holes via free-carrier absorption, enabling strongly enhanced nonlinear interactions.

The origin of the third nonlinearity enhancement can be described with a modified Drude model by introducing a non-simple harmonic scattering term as

$$\mathrm{m}^{*}\frac{d^{2}\vec{r}}{dt^{2}}+\mathrm{m}^{*}\frac{d\vec{r}}{dt}\gamma_{m}=\mathrm{q}\vec{E}e^{-i\omega t}+c.c. \tag{S10}$$

Where γ_m denotes the modified collision rate of the photoexcited electrons, which can be described as $\gamma_m=\frac{1}{\tau_0}+\beta\left(\frac{d\vec{r}}{dt}\right)^2$, τ_0 is the scattering time at low field, $\gamma=\frac{1}{\tau_0}$ denotes the collision rate of the electrons, β is the anharmonic coefficient representing the nonlinear influence of hot carriers, intervalley scattering, impact ionization, and Bloch oscillation. According to the definition of the modified collision rate, the equation (S10) can be written as

$$\mathrm{m}^{*}\frac{d^{2}\vec{r}}{dt^{2}}+\mathrm{m}^{*}\frac{d\vec{r}}{dt}\frac{1}{\tau_0}+\mathrm{m}^{*}\beta\left(\frac{d\vec{r}}{dt}\right)^{3}=\mathrm{q}\vec{E}e^{-i\omega t}+c.c. \tag{S11}$$

By assuming a general solution $\vec{r}=\vec{r}_{\omega}e^{-i\omega t}+\vec{r}_{3\omega}e^{-i3\omega t}$, and assuming the perturbative term and ignoring the higher-order terms, we can solve the solution of equation (S11) as

$$\vec{r}_{\omega}=\frac{q\vec{E}}{\mathrm{m}^{*}(\omega^{2}-i\omega\gamma)} \tag{S12}$$

Combining the equations (S12), the equation (S11) can be written as

$$\mathrm{m}^{*}\frac{d^{2}\vec{r}_{3\omega}}{dt^{2}}+\mathrm{m}^{*}\gamma\frac{d\vec{r}_{3\omega}}{dt}=-\mathrm{m}^{*}\beta\left(\frac{d\vec{r}_{\omega}}{dt}\right)^{3} \tag{S13}$$

According to the equation (S13), the motion with triple fundamental angular frequency can be solved as

$$\vec{r}_{3\omega}=\frac{i\beta\mathrm{q}^{3}\vec{E}\cdot\vec{E}\cdot\vec{E}}{\mathrm{m}^{*3}(9\omega^{2}-i3\omega\gamma)(\omega^{2}-i\omega\gamma)^{3}} \tag{S14}$$

According to the definition of the polarization density, the second-order polarization ($P_{3\omega}$) can be obtained as

$$P_{3\omega} = \frac{\oiiint_V \mathrm{q} n_e r_{3\omega} \mathrm{d}V}{V} \tag{S15}$$

Where n_e denotes the density of the photoexcited free electrons corresponding to the optical pump power, V denotes the volume of pumped GaAs, where has the third-order nonlinearity.

By assuming an average M times enhancement of the local electric field with respect to the incident THz electric fields.

$$p_{3\omega} = -\frac{iq^4 M^3 \langle n_e \rangle \beta E_i^3}{\mathrm{m}^{*3}(9\omega^2 - i3\omega\gamma)(\omega^2 - i\omega\gamma)^3} \tag{S16}$$

According to the definition of polarization density $P_{3\omega} = \varepsilon_0 \chi^{(3)} E_i \cdot E_i \cdot E_i$, where ε_0 denotes the vacuum permittivity, and $\chi^{(3)}$ denotes the effective second-order susceptibility.

$$\chi^{(3)} = -\frac{iq^4 M^3 \langle n_e \rangle \beta}{\varepsilon_0 \mathrm{m}^{*3}(9\omega^2 - i3\omega\gamma)(\omega^2 - i\omega\gamma)^3} \tag{S17}$$

While equation (S17) establishes that elevated carrier densities n_e enhance the third-order nonlinear coefficient $\chi^{(3)}$. However, the loss channels, such as predominantly free-carrier absorption and Auger recombination, become non-negligible at high excitation fluences. This introduces a critical trade-off, wherein $\chi^{(3)}$ follows a non-monotonic dependence on pump power. Consequently, maximizing the effective nonlinear response requires precise optimization of optical pumping intensity to operate at the global extremum of the third-order nonlinear coefficient $\chi^{(3)}$.

S2 Simulations of the THz metasurfaces

Simulation of the transmission spectrum

In this research, the finite-difference time-domain (FDTD) method is used to simulate the transmission spectrum of concept-of-proof metasurfaces. In the simulation, the high-resistance GaAs substrate is treated as having semi-infinite thickness with ε_{GaAs} = 12.9, and gold (Au) is modeled as a lossy metal with a conductivity of 4.1×10^7 S/m. To simulate the transmission spectrum, a single unit cell is simulated in the time domain with the periodic boundary condition in the x and y directions. To simulate the open space, we set the open boundaries on the bottom and top, respectively. Broadband y-polarized plane waves were implemented as excitation sources in finite-difference time-domain (FDTD) simulations. To quantify transmission characteristics, a field monitor recorded the y-component electric field transients at the GaAs substrate exit plane. Initial signal envelopes are isolated by applying a Hanning window to eliminate Fabry-Perot reverberations from substrate interfaces. Comparative simulations are performed for the metasurface and the unpatterned GaAs reference substrates.

Transmission spectra can be derived through the Fourier transformation of time-domain signals.

$$T(\omega)=\left|\frac{\mathrm{F}\{E_{\text{sample}}(t)\}}{\mathrm{F}\{E_{\text{reference}}(t)\}}\right| \tag{S18}$$

Where $T(\omega)$ denotes frequency-dependent transmittance normalized to the reference structure. $E_{\text{sample}}(t)$ and $E_{\text{reference}}(t)$ are the signals in the time domain of the metasurface and GaAs substrate, respectively.

Simulation of the second harmonic generation

To simulate the second harmonic generation caused by the Lorentz force, the commercial software COMSOL Multiphysics, based on the finite element method (FEM), is used to model and simulate the nonlinear properties of the proposed metasurface. The substrate materials used are high-purity GaAs. Then pumped GaAs film was modeled with conductivity and a thickness of 1 μm. The simulated results are shown in Figure S1. To simulate the magnetoelectric coupling effect in the pumped metasurface, an anisotropic conductivity tensor of the pumped GaAs is modeled as follows.

$$\tilde{\sigma}(B,\omega)=\tilde{\sigma}_0(\omega)\begin{pmatrix}\frac{1}{1+\beta^2} & -\frac{\beta}{1+\beta^2} & 0\\ \frac{\beta}{1+\beta^2} & \frac{1}{1+\beta^2} & 0\\ 0 & 0 & 1\end{pmatrix} \tag{S19}$$

where, $\beta(\omega)=\mu_e(\omega)\vec{B}_z(\omega)$, $\vec{B}_z(\omega)$ denotes the local magnetic field amplitude along the z-axis, $\tilde{\sigma}_0(\omega)$ and $\mu_e(\omega)$ denote the conductivity and at the fundamental angular frequency ω, respectively. The DC conductivity of the pumped-GaAs under a strong broadband THz pump is 640 $\text{S}\cdot\text{m}^{-1}$ and the mobility is 4200 $\text{cm}^2/\text{V}\cdot\text{s}$.

To simulate the second harmonic generation, a single meta-atom is simulated under time-domain excitation with Bloch-periodic boundaries along the x- and y-axis. The incident excitation is defined as a modulated plane wave with y polarization propagating along the z-axis, with its electric field component expressed as:

$$\vec{E}_{\text{i}}=|E_0|\cos\left(2\pi ft-kz\right)e^{-\left(\frac{t-t_d}{\Delta t}\right)^2} \tag{S20}$$

Where f denotes the fundamental frequency, t denotes the time, k denotes the wavenumber at the fundamental frequency, z denotes the coordinate in the z-axis, $|E_0|$ is the maximum amplitude of the incident THz field. Δt =5 ps, and t_d=15 ps are the parameters of the Gaussian pulse,

respectively.

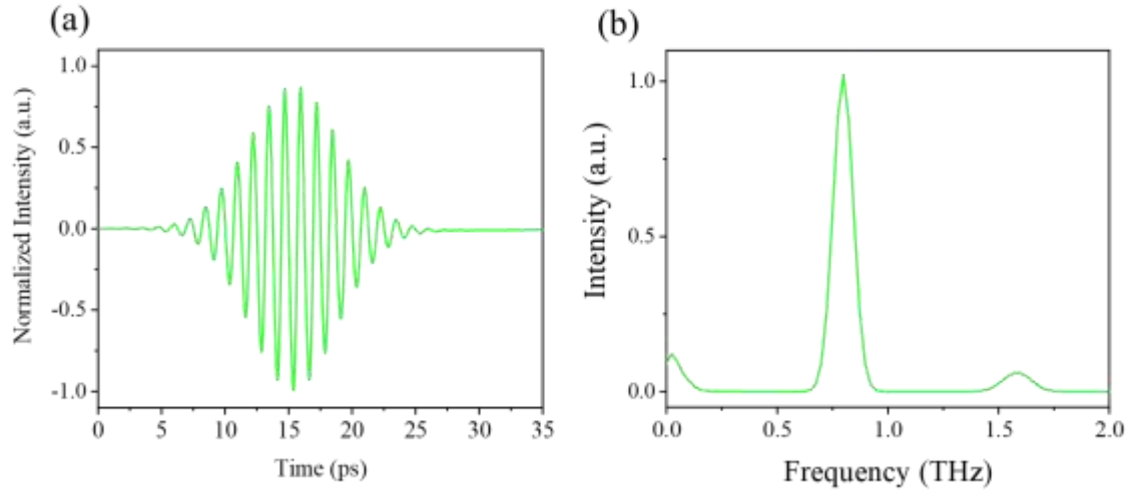

Figure S1 (a) The simulated time domain spectra of the THz SHG. (b) The simulated frequency domain spectra of THz SHG of the metasurfaces.

Simulation of the third harmonic generation

To simulate the third harmonic generation, a single unit cell is simulated in the time domain with periodic boundaries in the x and y axes, and the scattering boundaries are applied to the bottom and top boundaries, respectively. The y-polarized electric field of the incident wave is defined in the same way as the simulation of the second harmonic generation. Within the framework of nonlinear optics, third-harmonic generation is governed by the third-order nonlinear polarization:

$$P^{(3)}(3\omega) = \varepsilon_0 \chi^{(3)} E(\omega) E(\omega) E(\omega) \tag{S21}$$

Where, ε_0 denotes the permittivity in the vacuum, and $\chi^{(3)}$ denotes the third harmonic coefficient of the pumped GaAs, which is set as 3×10^{-13} m^2V^{-2}[1]. The simulated results can be seen in Figure S2.

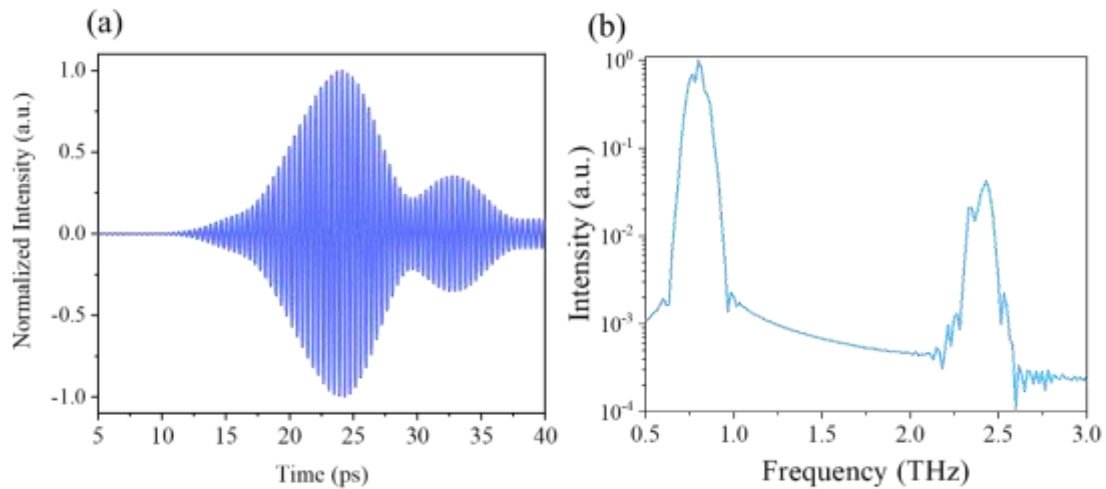

Figure S2 (a) The simulated time domain spectra of the THz THG. (b) The simulated frequency domain

spectra of THz THG of the metasurface.

S3 Experimental setup

To demonstrate the second- and third-harmonic generation properties in an experiment, we set up a tabletop pump-delay THz system at room temperature, as shown in **Figure S3a**. We employ a femtosecond laser amplifier to optically pump an organic crystal, 2-(3-(4-hydroxystyryl)-5,5-dimethylcyclohex-2-enylidene) malononitrile (OH1) to generate intense multi-cycle terahertz pulses. A ZnTe electro-optic crystal serves as the terahertz detector in the THz pump-delay-probe system, enabling time-resolved characterization of nonlinear harmonic generation and dynamic control. 80-fs pulses from a Ti: sapphire amplifier (Coherent Astrella, 1 kHz, 7 mJ) are split by a beam splitter. A 3.5 mJ portion of the split beam pumped an optical parametric amplifier (OPA), producing intense infrared pulses centered at 1550 nm via phase-matched difference-frequency generation. These mid-IR pulses subsequently drive optical rectification in a 1.5-mm-thick organic nonlinear crystal OH1, yielding high-field single-cycle terahertz radiation (In the linear transmission regime, the 1550 nm wavelength laser pulse energy was attenuated to approximately 0.15% of its original intensity using calibrated optical attenuators before excitation of the OH1 crystal). Terahertz pulses pass through a THz low-pass filter to attenuate residual infrared stray light.

The beam is then spectrally filtered by a custom-developed terahertz bandpass filter (BPF1) for fundamental frequency selection. The fundamental THz pulse in the time domain and frequency domain is shown in **Figure S3 b, c**, respectively. Collimated by a 2-inch focal length off-axis parabolic mirror (PM2), the filtered THz radiation is focused onto the harmonic-generation metasurface sample positioned near the parabolic mirror PM3. After interacting with the sample, which generates both fundamental and harmonic frequency components, the transmitted beam is collected and recollimated by the parabolic mirror PM3. A second custom bandpass filter (BPF2), positioned post-PM3, selectively transmitted either second or third-harmonic components by centering its passband at precisely twice or triple the fundamental frequency defined by BPF1, thereby rejecting residual fundamental radiation. Harmonic terahertz pulses generated by the metasurface are focused onto a <110>-oriented ZnTe electro-optic crystal via an off-axis parabolic mirror with central aperture (PM4). This induces instantaneous birefringence modulation in the crystal, with refractive index anisotropy proportionally tracking the terahertz electric field amplitude on femtosecond timescales. The polarization orientation of detected terahertz fields can be actively reconfigured by azimuthal rotation of the electro-optic crystal about the beam propagation axis, enabling polarization-selective measurements without realigning optical components.

The optical pump laser beam traversed a motorized delay stage (Delay Line 1) and passed through an optical chopper operating at 80 Hz for lock-in detection. Its fluence was precisely controlled via tunable neutral density filters before beam expansion through a Galilean telescope (Lens 1). The expanded beam was then directed onto the metasurface sample via an off-axis parabolic mirror with a central aperture, achieving spatial overlap with the terahertz focal spot. The relative temporal delay between pump and terahertz pulses was electronically scanned using Delay Line 1, which has a minimum step size of L_step = 0.03 mm, achieving a temporal resolution of ~0.2 ps, while pump power was dynamically adjusted through a calibrated attenuation system. The 800 nm wavelength pump beam was focused to a spot size of approximately 2 mm in diameter, which was significantly larger than the 1 mm diameter spot of the focused THz beam.

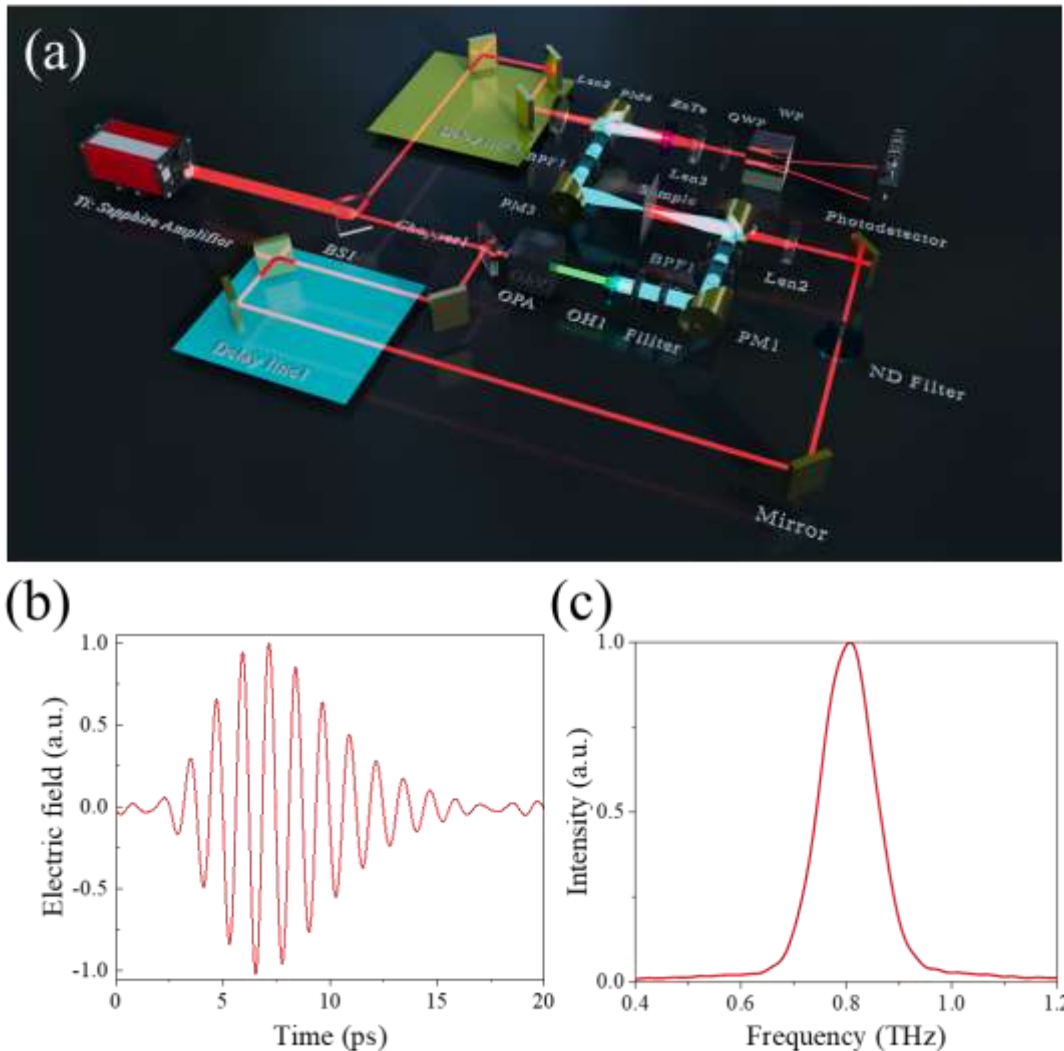

Figure S3 (a) The experimental set-up for the THz THG measurement. BS: Beam splitter; OPA: optical parametric amplifier; THz filter: low-pass filter with cut-off frequencies of 18 THz; PM1-4: Parabolic Mirror; BPF1: filters with center frequency at 0.8 THz with 15% bandwidth; BPF2: filters with center frequency at 1.6 THz (second harmonic) or 2.4 THz (third harmonic) with 15% bandwidth; TP: THz

polarizers; ND filter: neutral density filters; QWP: quarter wave plate; WP: Wollaston prism. The measured spectrum of the THz pump pulse with a fundamental frequency at 0.8 THz in the time domain (b), and frequency domain (c).

A probe laser beam (pulse energy <1 μJ, attenuated by neutral density filters) traversed a motorized delay stage (Delay Line 2) and is collimated by lens L1 before passing through the central aperture of parabolic mirror PM4. Propagating an equal optical path length as the THz generation arm, the probe pulse spatiotemporally overlapped with the terahertz radiation at the focal point on the ZnTe detector crystal. The probe is recollimated by len2 and passed through a quarter-wave plate (QWP) and Wollaston prism (WP), which orthogonally decomposes its polarization components. The beams are detected by the balanced photodetector. In the absence of THz excitation, the Wollaston prism split the probe into two equal-intensity beams, yielding a null differential signal. When the crystal experienced THz-induced birefringence, polarization rotation created an intensity imbalance between the decomposed beams. The resultant differential photocurrent scaled linearly with the instantaneous amplitude of the THz electric field. By scanning Delay Line 2, this system can map the temporal evolution of THz-driven refractive index anisotropy, enabling reconstruction of the terahertz spectral waveform. To eliminate the absorption of water vapor, the relative humidity of all measurements is kept below 5% by dry N_2 purging.

S4 The mechanisms of the dependence of SHG and THG on the optical pump energy density

Second harmonic generation

According to the equation (S9)

$$\chi^{(2)} \propto \langle n_e \rangle \langle \mu_e \rangle MN \tag{S22}$$

Moreover, the second-harmonic intensity scales quadratically with the amplitude of the second-order nonlinear polarization.

$$I_{2\omega} \propto \left| P_{2\omega} \right|^2 \propto \left| \chi^{(2)} \right|^2 \left| E_i \right|^4 \tag{S23}$$

By combining equation (S22) and equation (S23), the relationship between the intensity of SH can be described as

$$I_{2\omega} \propto (\langle n_e \rangle \langle \mu_e \rangle)^2 (MN)^2 \tag{S24}$$

Third harmonic generation

Under the relaxation-time approximation, the third-order nonlinear conductivity of a

semiconductor with parabolic energy bands can be rigorously derived from a simplified Boltzmann transport equation[2, 3].

The steady-state Boltzmann transport equation can be written as

$$\vec{v}\cdot\nabla_{\vec{r}}f+\frac{q}{\hbar}\vec{E}_i\cdot\nabla_{\vec{k}}f=\left(\frac{\partial f}{\partial t}\right)_{\text{coll}} \tag{S25}$$

Where, $\vec{v}$, q, $\hbar$, and $\vec{E}_i$ denote the velocity of the carrier, the elementary charge, the Planck constant, and the amplitude of the external electronic field, respectively. $\nabla_{\vec{r}}f$ and $\nabla_{\vec{k}}f$ are the gradient of the distribution function in the real space and moment space, respectively, where f is the non-equilibrium distribution function. $\left(\frac{\partial f}{\partial t}\right)_{\text{coll}}$ is the temporal rate of change of the distribution function.

Under the relaxation-time approximation, the steady-state Boltzmann transport equation can be simplified as

$$\vec{v}\cdot\nabla_{\vec{r}}f+\frac{q}{\hbar}\vec{E}\cdot\nabla_{\vec{k}}f=-\frac{f-f^{(0)}}{\tau} \tag{S26}$$

Where, $f^{(0)}$ is the equilibrium distribution function denoting the ultimate "rest state" of the system in the absence of any external perturbations. τ is the relaxation time.

By performing a Taylor expansion, the non-steady-state distribution function can be expressed as

$$\begin{aligned} f(\mathbf{k}) &= f^{(0)}(\mathbf{k})+\sum_{n=1}^{\infty}f^{(n)}(\mathbf{k}) \\ &\approx f^{(0)}(\mathbf{k})+f^{(1)}(\mathbf{k})+f^{(2)}(\mathbf{k})+f^{(3)}(\mathbf{k}) \end{aligned} \tag{S27}$$

Where, $f^{(\mathrm{n})}(\mathbf{k})$ denotes the nth order non-equilibrium distribution function, $\mathbf{k}$ denotes the momentum.

$$\frac{\partial f^{(\mathrm{n})}}{\partial t}+\frac{q}{\hbar}\vec{E}\cdot\nabla_{\vec{k}}f^{(n-1)}=-\frac{f^{(\mathrm{n})}}{\tau} \tag{S28}$$

For the 1st response can be described as

$$\left(-i\omega+\frac{1}{\tau}\right)f^{(1)}=-\frac{\mathrm{q}}{\hbar}\vec{E}_i\cdot\nabla_{\mathrm{k}}f^{(0)}. \tag{S29}$$

Due to the incident electronic field can be written as $\vec{E}_i=E_0e^{-i\omega t}+c.c.$, the solution of the equation (S29) can be solved.

$$f^{(1)}=-\frac{\mathrm{q}}{\hbar}\frac{\tau}{1-i\omega\tau}(\vec{E}_i\cdot\nabla_{\vec{k}}f^{(0)})e^{-i\omega t} \tag{S30}$$

By treating $\vec{E}_i \cdot \nabla_{\vec{k}} f^{(1)}$ as the driving term for $f^{(2)}$, substitution into the equation (S28)

$$\left(-i2\omega+\frac{1}{\tau}\right)f^{(2)}=-\frac{q}{\hbar}\vec{E}_i\cdot\nabla_{k}f^{(1)}. \tag{S31}$$

The $f^{(2)}$ can be described as

$$f^{(2)}=\left(\frac{q}{\hbar}\right)^2\frac{\tau^2}{(1-i2\omega\tau)(1-i\omega\tau)}\left[(\vec{E}_i\cdot\nabla_{\vec{k}})^2 f^{(0)}\right]e^{-i2\omega t} \tag{S32}$$

By treating $\vec{E}_i \cdot \nabla_{\vec{k}} f^{(2)}$ as the driving term for $f^{(3)}$, substitution into the equation (S28), we can get the expression for $f^{(3)}$ is

$$f^{(3)}(\vec{k},t)=-\left(\frac{q}{\hbar}\right)^3\frac{\tau^3}{(1-i3\omega\tau)(1-i2\omega\tau)(1-i\omega\tau)}\left[(\vec{E}_i\cdot\nabla_{\vec{k}})^3 f^{(0)}\right]e^{-i3\omega t} \tag{S33}$$

Since the relation between the current density, carrier velocity, and the probability distribution function can be expressed as

$$\vec{J}(t)=\frac{q}{V}\sum_{\vec{k}}\vec{v}(\vec{k})f(\vec{k},t)=\frac{q}{(2\pi)^d}\int d^d\vec{k}\vec{v}(\vec{k})f(\vec{k},t) \tag{S34}$$

Where, V denotes the volume, d is the dimension, and t is the time.

$$\vec{J}^{(3)}(t)=\frac{q}{(2\pi)^d}\int d^d\vec{k}\vec{v}(\vec{k})f^{(3)}(\vec{k},t) \tag{S35}$$

Combined the equation (S33), and for GaAs, the integral can be treated as $\langle n_e\rangle$ [4, 5]. The equation can be written as

$$J^{(3)}(t)=-\frac{q}{(2\pi)^d}\left(\frac{q}{\hbar}\right)^3\frac{n_e\tau^3E_i^3e^{-i3\omega t}}{(1-i3\omega\tau)(1-i2\omega\tau)(1-i\omega\tau)} \tag{S36}$$

According to the definition of the third order conductivity $\vec{J}^{(3)}(t)=\sigma^{(3)}(3\omega;\omega,\omega,\omega):\vec{E}_\omega\vec{E}_\omega\vec{E}_\omega e^{-i3\omega t}$, : denotes the contraction of the rank-four tensor $\sigma^{(3)}$.

$$\sigma^{(3)}\propto\frac{n_eq^4\tau^3}{\hbar^3(1-i3\omega\tau)(1-i2\omega\tau)(1-i\omega\tau)} \tag{S37}$$

Let $D(\omega)=(1-i3\omega\tau)(1-i2\omega\tau)(1-i\omega\tau)$

$$\sigma^{(3)}\propto\frac{q^4}{\hbar^3}\frac{\tau^3}{D(\omega)}\langle n_e\rangle \tag{S38}$$

Under the low-frequency approximation, the expression simplifies to[6]

$$\sigma^{(3)} \propto \langle n_e \rangle \tau^3 \tag{S39}$$

According to the definition of the carrier mobility $\mu_e = \frac{q\pi\tau}{m^*}$, m^* is the effective mass of the carrier.

$$\sigma^{(3)} \propto \langle n_e \rangle \langle \mu_e \rangle^3 \tag{S40}$$

According to the relationship $\chi^{(3)} = \frac{i\sigma^{(3)}}{\varepsilon_0 \omega}$, we can get the relationship between the intensity of THG and the third order conductivity as

$$I_{3\omega} = \left| \chi^{(3)} \cdot \mathrm{E_{loc}} \cdot \mathrm{E_{loc}} \cdot \mathrm{E_{loc}} \right|^2 \propto \langle n_e \rangle^2 \langle \mu_e \rangle^6 \tag{S41}$$

Furthermore, based on the empirically determined dependences of carrier density on pump fluence[7, 8], the quantity can be expressed as

$$n_e(P_{\mathrm{inc}}) = n_p \cdot \frac{P_{inc}}{1 + P_{inc} / P_0} \tag{S42}$$

Where, P_{inc}, and P_0 denote the incident pump energy density, and saturation pump energy density. n_p is the carrier-concentration proportionality coefficient.

The dependence of carrier mobility on the carrier density [9-11], can be described as

$$\mu_e(n_e) = \mu_{01} + \frac{\mu_{02}}{1 + (n_e / n_c)^{\varsigma}} \tag{S43}$$

Where, n_e, and n_c denote the carrier concentration, and critical carrier concentration. μ_{01} is the minimum mobility proportionality coefficient, μ_{02} is the difference between the maximum mobility and the minimum mobility proportionality coefficient. ς is the attenuation coefficient.

In addition, considering the influence of the conductivity on the local electric field enhancement coefficient *M* of the metasurface, it can be described as

$$M(\sigma) = \frac{M_0}{1 + (\sigma^{(1)} / \sigma_{\mathrm{M}})^{\mathrm{p}}} \tag{S44}$$

Where, M_0 is the maximum electric field enhancement factor, σ_{M} is the corresponding characteristic conductivity when the enhancement factor drops to half of its maximum value, p is the attenuation coefficient, and $\sigma^{(1)} = n_e \mu_e$ is the conductivity of the material.

The magnetic field enhancement coefficient *N* can be described as

$$N(\sigma) = \frac{N_0}{1 + (\sigma^{(1)} / \sigma_{\mathrm{N}})^{\mathrm{q}}} \quad \text{(S45)}$$

Where, N_0 is the maximum electric field enhancement factor, σ_{N} is the corresponding characteristic conductivity when the enhancement factor drops to half of its maximum value, and q is the attenuation coefficient.

Consequently, combing the equation (S24), and (S42)-(S46), we can obtain the pump-fluence-dependent expressions for the SHG and THG intensities as follows

$$\begin{aligned} I_{\mathrm{SHG}}(P_{inc}) &= A_{\mathrm{SHG}} \cdot [n_e \cdot \mu_e]^2 [(M(n_e, \mu_e) \cdot N(n_e, \mu_e)]^2 + C_{\mathrm{SHG}} \\ &= A_{\mathrm{SHG}} \cdot (\sigma^{(1)})^2 (M(n_e, \mu_e) \cdot N(n_e, \mu_e))^2 + C_{\mathrm{SHG}} \end{aligned} \quad \text{(S46)}$$

Where, A_{SHG}, and C_{SHG} are the amplitude coefficient of the second-harmonic generation, and the background offset of the SHG. $\sigma^{(1)}$ is the linear conductivity of the pumped GaAs. *M* and *N* is the local field enhancement factors of the electronic field and magnetic field, respectively.

$$\begin{aligned} I_{\mathrm{THG}}(P_{inc}) &= A_{\mathrm{THG}} \cdot n_e^{\,2} \cdot \mu_e^{\,6} M^6(n_e, \mu_e) + C_{\mathrm{THG}} \\ &= A_{\mathrm{THG}} \cdot [\sigma^{(1)}]^2 \cdot \mu_e^{\,4} M^6(n_e, \mu_e) + C_{\mathrm{THG}} \end{aligned} \quad \text{(S47)}$$

Where, A_{THG}, and C_{THG} are the amplitude coefficient of the third-harmonic generation, and the background offset of the THG.

Using equations (S46) and (S47), the normalized experimental data were fitted theoretically (For simplicity, $A_{\mathrm{THG}} = A_{\mathrm{SHG}} = 1$), the resulting correlation coefficients are listed in Table S1.

Table S1. Relative parameters of the dependence of the SHG and THG on the optical pump energy density

E_0 (μJ/cm²)	n_0	μ_{01}	μ_{02}
120	0.026	0	1.61
n_c	ς	A_THG	C_THG
3.2	0.9	1	0
A_SHG	C_SHG	M_0	σ_M
1	-0.1	1.9	0.3
p	N_0	σ_N	q
1	3.69	0.82	1

S5 Second and third-order susceptibility

Second-order susceptibility

The efficiency of SHG based on pumped THz nonlinear metasurfaces can be described as

$$\mathrm{P}_{\mathrm{SHG}} = \frac{(4\pi f)^2 (\chi_{\mathrm{eff}}^{(2)})^2 d^2}{\varepsilon_0 c^3 n_\omega^2 n_{2\omega}} I_0^2 A \tag{S48}$$

Where, $\mathrm{P}_{\mathrm{SHG}}$ denotes the power of the second harmonic, $\chi_{\mathrm{eff}}^{(2)}$ effective third-order susceptibility d=1.0 μm is the thickness of the pumped GaAs film, n_{2f} =3.51 denotes the refractive index of GaAs at the second harmonic frequency, $\boldsymbol{c}$ denotes the speed of light, I_0 denotes the incident THz fundamental field intensity, and A denotes the total area of the metasurfaces illuminated by THz fundamental field.

According to the equation (S48), the $\chi_{\mathrm{eff}}^{(2)}$ can be written as

$$\left|\chi_{\mathrm{eff}}^{(2)}\right| = \frac{|E_{\mathrm{SHG}}| 2c_0 n_{2f}}{|E_{\mathrm{i}}|^2 2\pi f d} \tag{S49}$$

Where, E_{2f} and E_{i} are the peak amplitudes of the generated third harmonic field and incident fundamental field, respectively.

Third-order susceptibility

The power of the third harmonic from pumped THz nonlinear metasurfaces can be described as

$$\mathrm{P}_{\mathrm{THG}} = \left(\frac{3 \times 2\pi f \chi_{\mathrm{eff}}^{(3)} d}{4\varepsilon_0 {n_{3f}}^2 c^2} \right)^2 I_0^3 A \tag{S50}$$

Where, $\mathrm{P}_{\mathrm{THG}}$ denotes the power of the third harmonic, $\chi_{\mathrm{eff}}^{(3)}$ effective third-order susceptibility d=1.0 μm is the thickness of the pumped GaAs film, n_{3f} =3.6 denotes the refractive index of GaAs at the third harmonic frequency, $\boldsymbol{c}$ denotes the speed of light, I_0 denotes incident THz fundamental field intensity, and A denotes the total area of the metasurface illuminated by the THz fundamental field.

According to the equation (S50), the $\chi_{\mathrm{eff}}^{(3)}$ can be written as

$$\left|\chi_{\mathrm{eff}}^{(3)}\right| = \frac{|E_{3f}| \cdot 4c \cdot n_{3f}}{|E_{\mathrm{i}}|^3 \cdot 3\pi f d} \tag{S51}$$

Where, E_{3f} and E_{i} are the peak amplitudes of the generated third harmonic field and incident fundamental field, respectively.

S6 Intervalley scattering

To quantitatively model the inter-valley redistribution of non-equilibrium electrons within the conduction band of pumped GaAs under intense THz fields, the transient electron population in the Γ valley can be described as

$$\frac{\mathrm{d}n_{\Gamma}(t)}{\mathrm{d}t} = -\gamma_{\Gamma L}(t)\, n_{\Gamma}(t) + \gamma_{L\Gamma}\left(n_0 - n_{\Gamma}(t)\right) \tag{S52}$$

Where, $\gamma_{\Gamma L}$ and $\gamma_{L\Gamma}$ denote the scattering rate from the Γ valley to the L valley and from the L valley to the Γ valley, respectively, n_{Γ} and n_{Γ} denote the carrier density of the Γ valley and L valley, respectively. t denotes the time, n_0 is the total carrier density of the pumped GaAs, which can be assumed to be a constant because of the long lifetime of photoexcited electrons in GaAs. $\gamma_{L\Gamma}$ can be assumed to be a constant, while $\gamma_{\Gamma L}$ is strongly dependent on the kinetic energy of electrons[12].

According to the band structure of GaAs, electron mobilities for satellite valleys are smaller than those for the main valley [13]. Therefore, the total drift current density is governed mostly by the electrons in the main valley. The hole drift current density can be assumed to be negligible because of the low mobility of holes in GaAs[14]. For simplicity, $|v_{\Gamma}(t)|$ is assumed to be determined by only the electron drift. We can describe the $\gamma_{\Gamma L}$ as a function of the electron drift velocity $|v_{\Gamma}(t)|$.

$$\gamma_{\Gamma L}(t) = \begin{cases} 0, & |v_{\Gamma}(t)| < v_{\mathrm{th}} \\ \gamma_{\Gamma \mathrm{L}}\sqrt{1+\left(\dfrac{|v_{\Gamma}(t)| - v_{\mathrm{th}}}{v_s}\right)^2} - 1, & |v_{\Gamma}(t)| \geq v_{\mathrm{th}} \end{cases} \tag{S53}$$

where v_{th} and v_{s} are the threshold velocity, and the saturation drift velocity, respectively. The inter-valley occurs when the electron drift velocity $|v_{\Gamma}(t)|$ exceeds the threshold velocity v_{th}.

The thermal energy from a room-temperature environment (~ 26 meV) is negligible compared with the kinetic energy from the electron drift. Given the shallow optical penetration depth of the pump beam and limited carrier diffusion length in GaAs, the photoactivated conductive region presents a sub-wavelength thickness profile, negligible compared to the incident terahertz wavelength with lower optical pump[15, 16]. The attenuation of the photoexcited region to the transmitted intense THz field can be ignored. The THz field in GaAs can be estimated to be $\frac{2FE_{\mathrm{i}}(t)}{1+\mathrm{n}_{GaAs}}$, where F denotes the field enhancement factor of the metasurfaces structure and $\mathrm{n}_{\mathrm{GaAs}}$

is the refractive index of GaAs. According to the Drude model and the definition of the incident intense THz field in equation (S20), the drift velocity determined by the incident THz field can be described as

$$v_{\Gamma}(t)=\frac{2F\mu_{\Gamma 0}}{(1+\mathrm{n}_{\mathrm{GaAs}})\sqrt{1+\omega^2\tau_{\Gamma}^2}}E_0 e^{-\left(\frac{t-t_0}{\Delta t}\right)^2}\cos(2\pi ft-\varphi) \tag{S54}$$

Where, $\mu_{\Gamma 0}$ and τ_{Γ} are the mobility of dc mobility and relaxation time of electrons in the Γ valley, respectively.

The relationship of DC mobility and relaxation time can be described as the following relation

$$\mu_{\Gamma 0}=\frac{\mathrm{q}\pi\tau_{\Gamma}}{\mathrm{m}^*} \tag{S55}$$

Where, where q is the elementary charge, m* is the effective mass of the electron in the Γ valley of GaAs.

Table S2. Parameters used for the calculation of intervalley scattering illuminated by THz wave[12]

$\gamma_{L\Gamma}$ [THz]	v_{th} [m·s^{-1}]	v_{s} [m·s^{-1}]	$\mu_{\Gamma 0}$ [m^2·V^{-1}·s^{-1}]	$\mathrm{n}_{\mathrm{GaAs}}$	M^*_{Γ}
0.53	2×10^5	1×10^5	0.4	3.59	0.067m$_e$

Leveraging the parameters tabulated in Table S2, we numerically computed electron populations within the Γ and L valleys of pumped GaAs. $n_{\Gamma}(t)$ can be determined by solving Equations (S53-S55) as shown in Under the premise of neglecting terahertz-field-induced metasurface resonance shifts and spatial field inhomogeneities, a homogenized field enhancement factor of *F* = 4.0 is adopted. The intervalley redistribution phenomena in the pumped GaAs metasurface subjected to terahertz peak fields of 5.0 kV/cm, 10.0 kV/cm, and 20.0 kV/cm are shown in Figure S4.

With a weak THz field, intervalley scattering has a weak effect, and all carriers almost remain in the Γ valley. As the incident THz field increases, the energy of carriers in the Γ valley gradually increases, causing them to scatter into the L valley.

At low field strengths, carriers remain almost entirely confined within the Γ valley due to insufficient kinetic energy for intervalley transfer. With intense field strength, progressive carrier energization in the Γ valley triggers scattering into higher-energy L valleys.

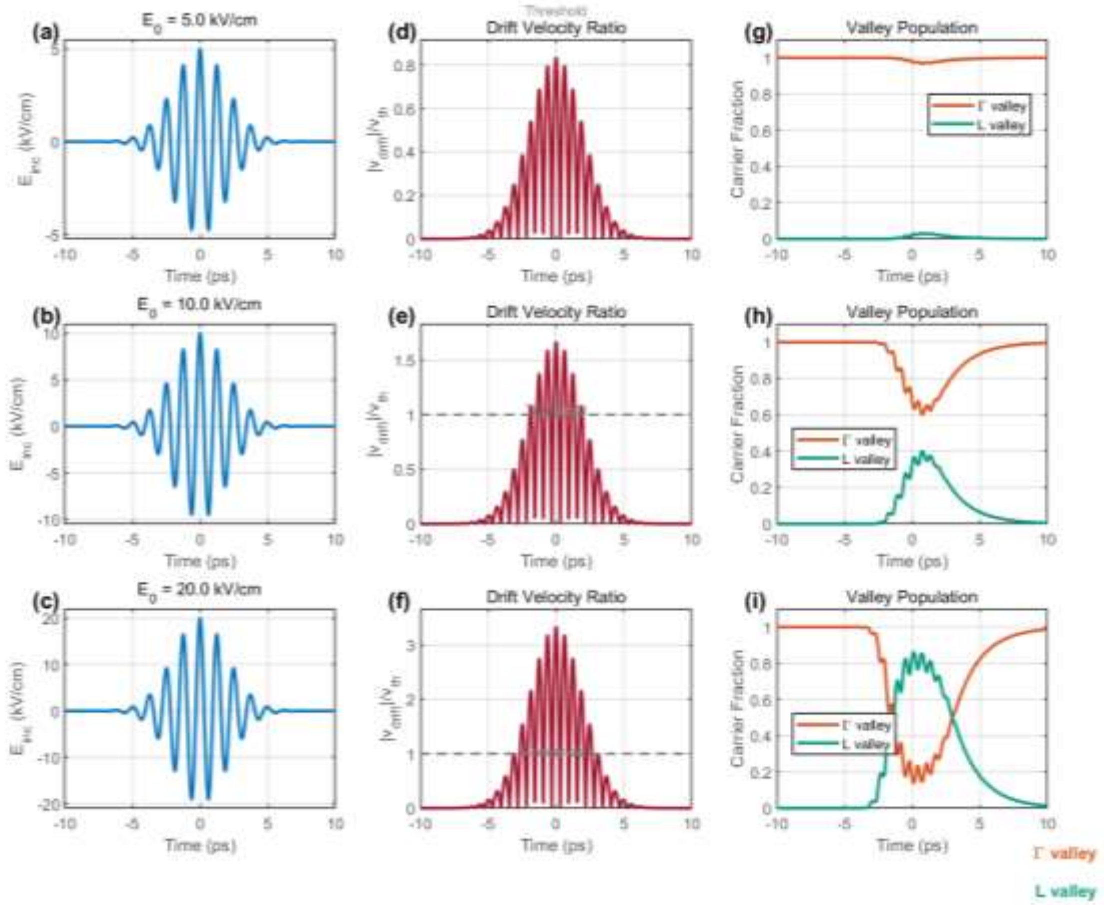

Figure S4 (a-c) Multicycle fundamental THz waves with different amplitudes. (d-f) The drift velocity ratio under THz waves with different amplitudes. (g-i) Carrier densities in the Γ and L valleys of pumped GaAs.

S7 The influence of thermal accumulation

The influence of the rise of temperature under an 800 nm wavelength laser can be made using the one-dimensional heat diffusion formula:

$$\Delta T = \frac{F(1-R)}{\rho C d}, \tag{S56}$$

where F is the fluence (50 μJ cm^{-2}), R is the surface reflectivity (~0.3 for GaAs at 800 nm wavelength), ρ is the material density (5.32 g/cm^3), C is the volumetric heat capacity (~1.8 J cm^{-3} K^{-1}), d is the optical absorption depth (~1 μm) [17-19].

The transient temperature rise per pulse can be calculated as

$$\Delta T = \frac{4.1\times10^5}{5.32\times10^3\times330} \approx 0.24\text{K}. \tag{S57}$$

The subsequent thermal diffusion time is estimated as

$$\tau_{\text{th}} = \frac{d^2}{D} = \frac{d^2\rho c}{k}, \tag{S58}$$

where D and k denote the thermal diffusivity and thermal conductivity (46 W/(m·K)) of the material, respectively.

The thermal diffusivity and thermal conductivity of the material can be described as

$$D = \frac{k}{\rho c} = \frac{46}{5.32\times10^{3}\times330} = 2.6\times10^{-5}\,\mathrm{m}^2/\mathrm{s}, \tag{S59}$$

$$\tau_{\mathrm{th}} = \frac{d^2}{D} = \frac{(1\times10^{-6})^2}{2.6\times10^{-5}} \approx 3.8\times10^{-8}\,\mathrm{s} = 38\mathrm{ns}. \tag{S60}$$

Since the repetition rate of the laser is 1 kHz (pulse interval = 1 ms), the thermal diffusion time is shorter than the pulse interval. Therefore, the deposited heat dissipates completely before the arrival of the next pulse, and no cumulative heating occurs.

References

1. Lee K, Park J, Kang BJ *et al.* Electrically controllable terahertz second-harmonic generation in GaAs. *Adv Opt Mater*. 2020; **8**(18). doi: 10.1002/adom.202000359
2. Kuznetsov AV, Stanton CJ. Theory of coherent phonon oscillations in semiconductors. *Phys Rev Lett*. 1994; **73**(24): 3243-3246. doi: 10.1103/PhysRevLett.73.3243
3. Haug H, Koch SW. *Quantum theory of the optical and electronic properties of semiconductors*. World Scientific, 2009.
4. Nilsson NG. Empirical approximations for the Fermi energy in a semiconductor with parabolic bands. *Appl Phys Lett*. 1978; **33**(7): 653-654. doi: 10.1063/1.90452
5. Gao Y, Zhang Z-Q, Ding K-H. Third-order nonlinear Hall effect in two-dimensional Dirac systems. *New Journal of Physics*. 2023; **25**(5): 053013. doi: 10.1088/1367-2630/acd2f8
6. Mayer A, Keilmann F. Far-infrared nonlinear optics. II. Chi3 contributions from the dynamics of free carriers in semiconductors. *Phys Rev B*. 1986; **33**(10): 6962-6968. doi: 10.1103/PhysRevB.33.6962
7. Shah J. Cooling of Hot Carriers. In: Shah J (ed.). *Ultrafast Spectroscopy of Semiconductors and Semiconductor Nanostructures*. Berlin, Heidelberg: Springer Berlin Heidelberg; 1999. 161-192.
8. Pankove JI, Kiewit DA. Optical Processes in Semiconductors. *J Electrochem Soc*. 1972; **119**(5): 156Ca. doi: 10.1149/1.2404256
9. Nag B. Scattering Theory. In: Nag B (ed.). *Electron Transport in Compound Semiconductors*. Berlin, Heidelberg: Springer Berlin Heidelberg; 1980. 93-128.
10. Jacoboni C, Reggiani L. The Monte Carlo method for the solution of charge transport in semiconductors with applications to covalent materials. *Reviews of Modern Physics*. 1983; **55**(3): 645-705. doi: 10.1103/RevModPhys.55.645
11. Masetti G, Severi M, Solmi S. Modeling of carrier mobility against carrier concentration in arsenic-, phosphorus-, and boron-doped silicon. *IEEE Trans Electron Devices*. 1983; **30**(7): 764-769. doi: 10.1109/T-ED.1983.21207
12. Hebling J, Hoffmann MC, Hwang HY *et al.* Observation of nonequilibrium carrier distribution in Ge, Si, and GaAs by terahertz pump--terahertz probe measurements. *Phys Rev B*. 2010; **81**(3): 035201. doi: 10.1103/PhysRevB.81.035201
13. Al-Ammar KH. Electronic structure of Gallium Arsenide under pressure. In: *2012*.
14. Katzenellenbogen N, Grischkowsky D. Electrical characterization to 4 THz of N - and P - type

GaAs using THz time - domain spectroscopy. *Appl Phys Lett*. 1992; **61**(7): 840-842. doi: 10.1063/1.107762 %J Applied Physics Letters

15. Aspnes DE, Kelso SM, Logan RA *et al.* Optical properties of AlxGa1−x As. *J Appl Phys*. 1986; **60**(2): 754-767. doi: 10.1063/1.337426 %J Journal of Applied Physics
16. Chang Y-M, Chang N-A. Coherent longitudinal optical phonon and plasmon coupling in GaAs. *Appl Phys Lett*. 2002; **81**(20): 3771-3773. doi: 10.1063/1.1521246 %J Applied Physics Letters
17. Potter RF. Chapter 2 - Basic Parameters for Measuring Optical Properties. In: Palik ED (ed.). *Handbook of Optical Constants of Solids*. Burlington: Academic Press; 1997. 11-34.
18. CRC Handbook of Chemistry and Physics: A Ready-Reference of Chemical and Physical Data, 85th ed Edited by David R. Lide (National Institute of Standards and Technology). CRC Press LLC: Boca Raton, FL. 2004. 2712 pp. $139.99. ISBN 0-8493-0485-7. *J Am Chem Soc*. 2005; **127**(12): 4542-4542. doi: 10.1021/ja041017a
19. Aspnes DE, Studna AA. Dielectric functions and optical parameters of Si, Ge, GaP, GaAs, GaSb, InP, InAs, and InSb from 1.5 to 6.0 eV. *Phys Rev B*. 1983; **27**(2): 985-1009. doi: 10.1103/PhysRevB.27.985